

# UC Santa Barbara

## UC Santa Barbara Previously Published Works

### Title

Lattice relaxations around individual dopant atoms in SrTiO<sub>3</sub>

### Permalink

<https://escholarship.org/uc/item/7g6455s3>

### Journal

Physical Review Materials, 3(11)

### ISSN

2475-9953

### Authors

Salmani-Rezaie, Salva  
Kim, Honggyu  
Ahadi, Kaveh  
[et al.](#)

### Publication Date

2019-11-08


### DOI

10.1103/PhysRevMaterials.3.114404

Peer reviewed

## Lattice relaxations around individual dopant atoms in SrTiO<sub>3</sub>

Salva Salmani-Rezaie, Honggyu Kim, Kaveh Ahadi, and Susanne Stemmer\*  
 Materials Department, University of California, Santa Barbara, California 93106–5050, USA

 (Received 3 July 2019; revised manuscript received 22 September 2019; published 8 November 2019)

The local atomic structure around individual dopant atoms can directly influence the electronic properties of a doped material. Here, we use quantitative scanning transmission electron microscopy to study the local lattice relaxations around Sm dopant atoms in SrTiO<sub>3</sub> thin films. These films have recently been shown to undergo successive ferroelectric and superconducting transitions when strained. We show that neighboring Ti-O columns move away from the columns that contain Sm dopants. The observed displacements are, however, more complex than a simple outward expansion of all four surrounding Ti-O columns. We discuss potential implications, especially for the ferroelectric transition observed in strained films.

DOI: [10.1103/PhysRevMaterials.3.114404](https://doi.org/10.1103/PhysRevMaterials.3.114404)

### I. INTRODUCTION

Doped SrTiO<sub>3</sub> exhibits a wide range of remarkable properties. For example, SrTiO<sub>3</sub> exhibits a “superconducting dome” as a function of carrier density [1]. Recently, doped SrTiO<sub>3</sub> has been found to undergo successive ferroelectric and superconducting transitions [2–5]. Other unique properties include an extraordinarily large Bohr radius that causes metallic conduction and superconductivity to persist to very low carrier densities [6,7] and a mobile carrier scattering rate that has a quadratic temperature dependence even far outside the Fermi liquid regime [8–12]. The origin of many of these phenomena remains a subject of considerable debate in the literature and suggest a need for an improved, atomic-scale understanding of doped SrTiO<sub>3</sub>.

Dopant atoms affect not only the electronic properties but also the local atomic structure in their vicinity. These local lattice relaxations can directly influence the electrical properties. For example, atomic displacements around the famous “DX centers” in semiconductors are responsible for transforming donors into acceptors [13]. The nature of dopant-induced structural changes are, however, often poorly understood. For example, Janotti *et al.* [14] found substantial discrepancies between density functional theory (DFT) calculations of the lattice parameter expansion of SrTiO<sub>3</sub> with doping and the corresponding experimental values. The discrepancy could not be explained by the size mismatch between the dopant and the host or the inverse deformation potential effect (a deformation in response to the presence of mobile charge in the conduction band [15]), both of which were taken into account in the calculations. Similarly, the local atomic configuration around Sr vacancies in SrTiO<sub>3</sub>, imaged by quantitative scanning transmission electron microscopy (Q-STEM [16]), was found to be substantially different from DFT predictions [17]. These discrepancies show that it is necessary to develop experimental methods that can determine the local atomic structure changes associated with dopant atoms.

Q-STEM is a powerful technique that allows for determining the three-dimensional location of individual dopant

atoms [18–22] and local column displacements [17,23,24]. For example, in combination with image registration methods, picometer displacements around individual Sr vacancies in SrTiO<sub>3</sub> could be resolved [17]. Compared to vacancies, substitutional atoms likely cause smaller disturbances of the surrounding lattice and are therefore more challenging to detect. In this study, we use Q-STEM to show that Ti-O columns around Sm dopant atoms are displaced relative to their positions in undoped SrTiO<sub>3</sub>. We show that the displacements are more complicated than those around Sr vacancies and discuss the potential implications for the properties of these films.

### II. EXPERIMENTAL

250-nm-thick, Sm-doped SrTiO<sub>3</sub> films were grown on (001) SrTiO<sub>3</sub> single crystals using hybrid molecular beam epitaxy [25,26]. The Sm concentrations, estimated from the mobile carrier densities, were 2% and 3%, respectively. An undoped SrTiO<sub>3</sub> film served as a reference. Similar to La-doped films [14], the lattice parameter systematically increased with increasing concentration of Sm. For undoped films, x-ray diffraction showed the expected lattice parameter of 3.905 Å, while films with 2% and 3% Sm had lattice parameters of 3.9105 and 3.912 Å, respectively. Plan-view TEM samples were prepared by mechanical wedge polishing with a 1.5° angle. High-angle annular dark-field (HAADF) STEM images were recorded along ⟨100⟩ using a FEI Titan S/TEM ( $C_s = 1.2$  mm) operating at 300 keV with a semi-convergence angle of 9.6 mrad. A HAADF detector angular range of 60–390 was selected by choosing a camera length of 100 cm. To improve the signal-to-noise ratio and minimize scan distortions, 20 fast-scan images were recorded, cross-correlated, and then averaged [17]. Position averaged convergent beam diffraction (PACBED) patterns [27], shown in the Supplemental Material [28], were used to reduce the sample tilt to less than 1 mrad from the zone axis, which is important to minimize artifacts in the measured displacements [29]. Absolute column intensities, referenced to the incident beam intensity [16,30,31], were determined by averaging over a circular region with a radius corresponding to a quarter of the lattice constant of SrTiO<sub>3</sub>. The integrated

\*Corresponding author: stemmer@mrl.ucsb.edu

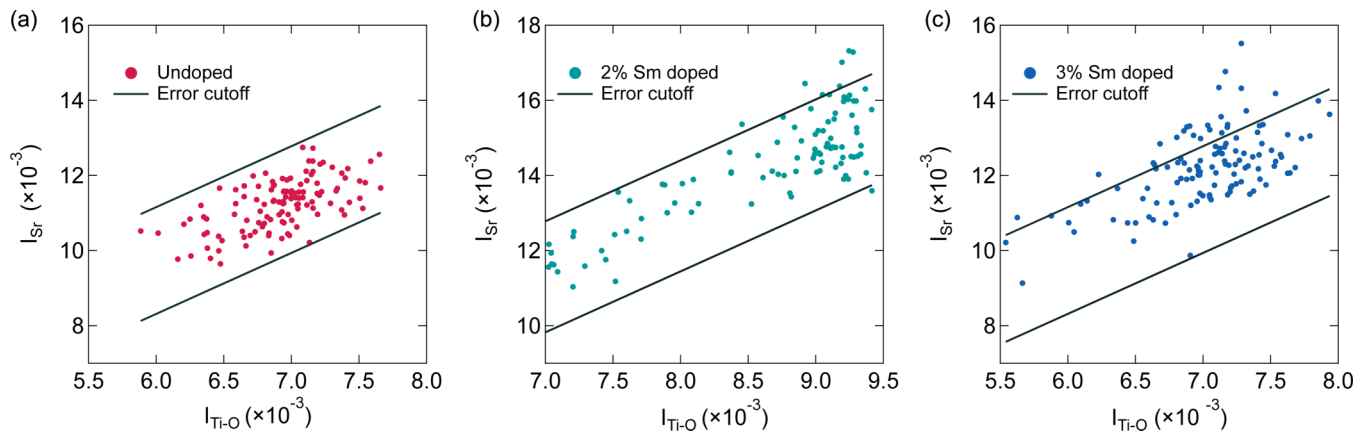


FIG. 1. Experimental  $I_{\text{Sr}}$  as a function of  $I_{\text{Ti-O}}$  for the (a) undoped (b) 2% Sm-doped, and (c) 3% Sm-doped  $\text{SrTiO}_3$ . Points that they lie above the experimental cutoff contain Sm. With increasing Sm concentration, more data points lie above the cutoff.

scattering cross section is robust against experimental parameters such as defocus, convergence angle, integration area, and source coherence [32]. Column positions were determined by iterative fitting to a two-dimensional Gaussian function. The Kirkland multislice algorithm [33] was used to simulate HAADF-STEM images using the frozen phonon method. The procedure used for estimating the number of Sm dopants in each column and their positions is described in Refs. [18,19]. It includes determining the experimental noise and error using the undoped  $\text{SrTiO}_3$  film, which establishes a visibility criterion for detecting dopant atoms [18,19]. Additional details can be found in the Supplemental Material [28].

### III. RESULTS AND DISCUSSION

Figure 1 shows experimental Sr column intensities ( $I_{\text{Sr}}$ ) extracted from three representative images of the undoped, 2% Sm-doped, and 3% Sm-doped  $\text{SrTiO}_3$  films, respectively. They are shown as a function of the intensity of the four Ti-O columns surrounding each Sr column ( $I_{\text{Ti-O}}$ ). The Ti-O columns do not contain Sm and therefore serve as a local measure of the foil thickness. The dark lines indicate our measure of the experimental error, taken to be the full width half maximum of the normal distribution of the experimental data points of the undoped sample [Fig. 1(a)]. For the doped samples, Sr columns with intensities above the upper error bound contain Sm, which has a higher atomic number than Sr. With increasing Sm concentration, the distribution of column intensities shifts upwards and more data points lie outside the error cutoff, consistent with the fact that more Sr columns contain Sm. We note that the experimental cutoff chosen here appears to be too conservative, especially for thinner regions, as can also be seen from larger data sets shown in the Supplemental Material [28]. This does not affect the analysis in the following.

Figures 2(a)–2(c) show displacement maps for the Ti-O columns overlaid on the images that were analyzed in Fig. 1. The displacement vectors (yellow arrows) show the difference between the actual position of the Ti-O columns, obtained by Gaussian peak fitting, and the center of mass of the four surrounding Sr columns. For clarity, the displacement vectors are shown magnified by a factor of six. Increasing the dopant concentration results in the presence of larger displacements

(for histograms of the displacement vectors, see the Supplemental Material [28]). An alternative way of visualizing the Ti-O column displacements is color contour maps of displacement vectors, shown in Figs. 2(d)–2(f). Increasing the dopant concentration results in a larger number of columns that have displacements significantly above the average displacement of the undoped sample (red color).

Sources of noise, image distortions, small residual sample tilt, and, possibly, real sources of disorder (defects) lead to the presence of apparent displacements even in the undoped film. The displacements found in the undoped samples were comparable to those in  $\text{SrTiO}_3$  reported in the literature [29]. We therefore defined an experimental error cutoff corresponding to the largest displacement found in the undoped sample (see Supplemental Material [28]). Figure 3(a) shows the displacement vector map for the sample with 3% Sm, where the displacement vectors that have a magnitude greater than this cutoff value are indicated by the small (light blue) squares. Two representative columns (labeled A and B) that contain Sm, as determined from the intensity maps, are highlighted by the red and purple squares and are magnified in Figs. 3(b) and 3(d). The corresponding Sr column intensity maps are shown in Figs. 3(c) and 3(e). Both columns each contain two Sm dopants, but at different depth positions (see Supplemental Material for details [28]). Additional results, including for the 2% sample, are shown in the Supplemental Material [28]. In general, we found that the Ti-O columns tend to displace away from the Sm dopants in both films. Interestingly, no displacement vectors with a magnitude greater than the error cutoff were found that pointed toward the Sm-containing Sr columns. As can be seen from Figs. 3(b) and 3(d), the displacement vector fields are, however, more complicated than a simple, uniform, outward displacements of the four Ti-O columns away from the Sm-containing Sr columns. We note that although the measured displacements are projected in the image plane, image simulations show displacements even if only the Ti-O atoms next to the Sm dopant displace (rather than the entire Ti-O column). Furthermore, there is a linear relation between the actual displacement and the measured displacement [28]. While the exact configuration of displaced columns along the depth direction cannot be determined in the experiments, variable angle quantitative Q-STEM may potentially provide this information [19].

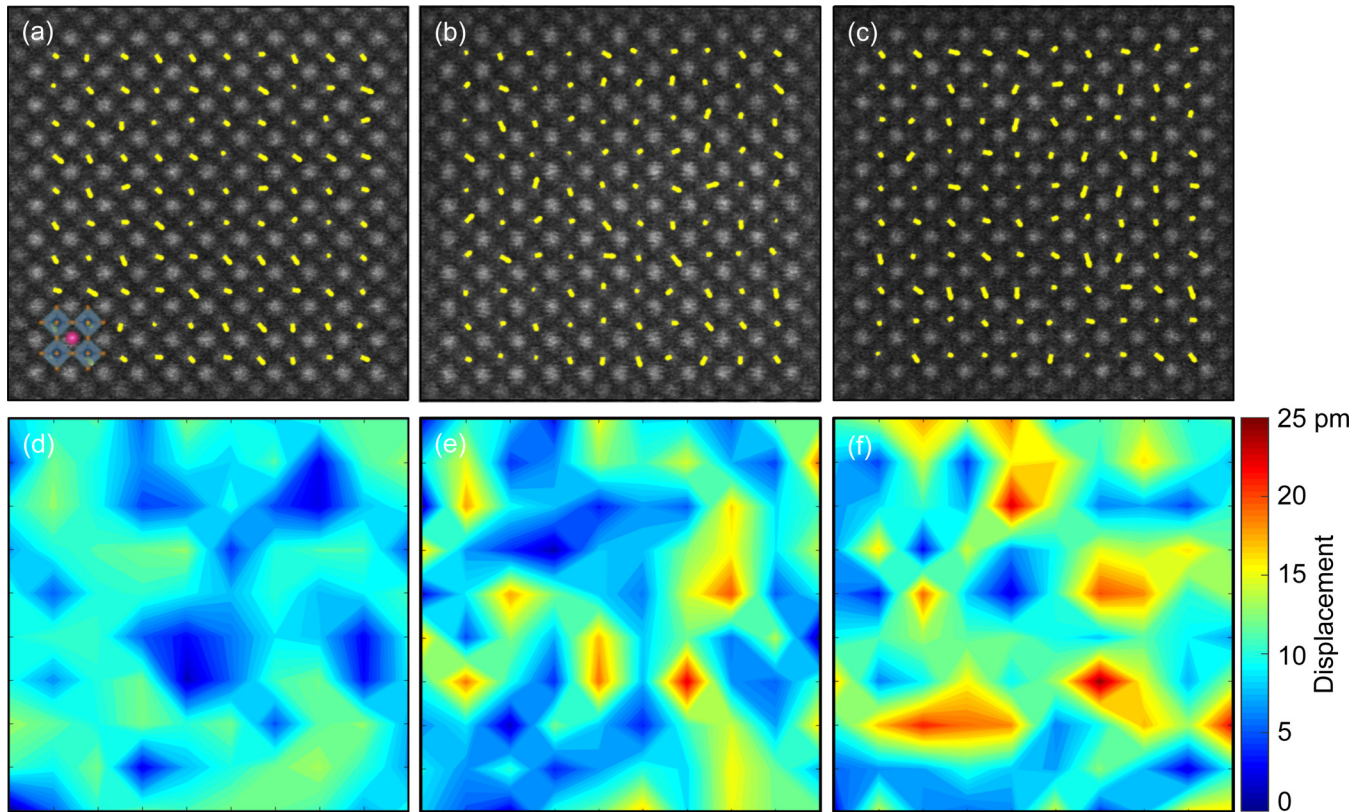


FIG. 2. Ti-O column displacements for the three samples. (a)–(c) HAADF-STEM images (same as analyzed in Fig. 1) of (a) undoped, (b) 2% Sm-doped, (c) 3% Sm-doped films with the displacement vectors for the Ti-O columns overlaid. The lengths of the vectors are depicted six times larger than the actual values. (d)–(e) Color contour maps of the displacement vectors for (d) undoped, (e) 2% Sm-doped, and (f) 3% Sm-doped  $\text{SrTiO}_3$ .

The displacement of the Ti-O columns away from the Sm dopants is not a size effect, because the effective ionic radius of the  $\text{Sm}^{3+}$  dopant (1.24 Å) is smaller than that of the  $\text{Sr}^{2+}$

(1.44 Å) it replaces, and is therefore electronic in origin. It is also different from the uniform expansion predicted in DFT calculations for La dopants in  $\text{SrTiO}_3$  [34]. One possible

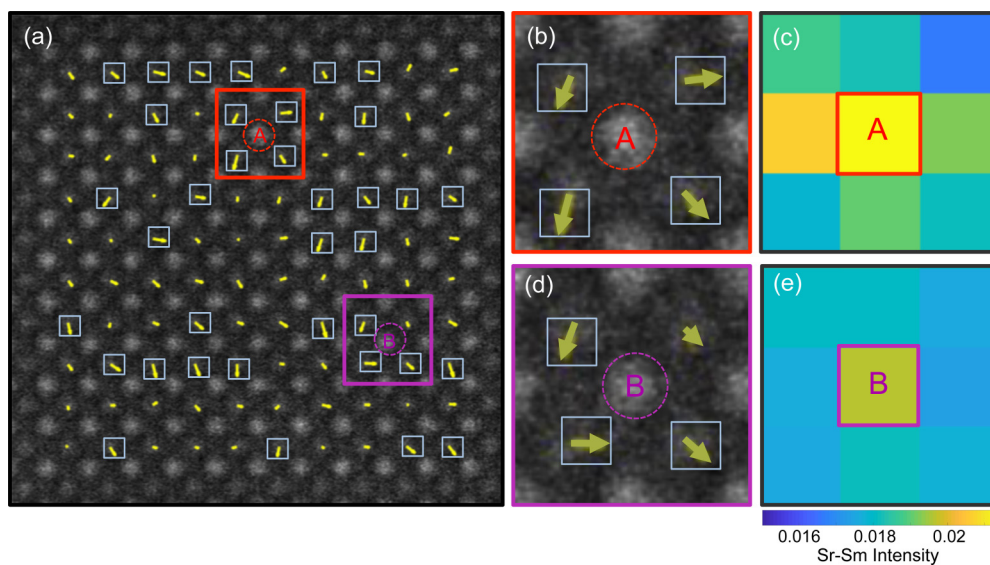


FIG. 3. (a) Image and displacement vectors for the sample with 3% Sm [same as Fig. 2(c)]. Vectors with displacements that are above the error cutoff are highlighted by small (light blue) squares. (b), (d) Ti-O column displacements of the red and purple regions highlighted in (a), which surround columns A and B, respectively. Sr column intensity maps around columns A and B are shown in (c) and (d), respectively. The high intensity indicates the presence of Sm.



reason is the high density of dopant atoms in the samples investigated here, which may result in overlapping strain fields. It would be interesting to perform DFT calculations for this case. The random, local nature of the displacements are, however, qualitatively similar even in regions where the dopant-containing columns spaced further apart (see, e.g., Figs. 3 and S5 [28]). Furthermore, Sm, unlike La, has  $f$  electrons, whose electronic coupling to the conduction band states may play a role in the local atomic configuration. A more complex defect configuration should also be considered. For example, DFT calculations show that Schottky defects cause more complicated and random outward/inward displacements [34]. The presence of Schottky defects seems, however, unlikely here, since the Sm dopants act as donors and are thus not compensated by Sr vacancies. Furthermore, our previous study has shown that Sr vacancies can be detected in the images [17]. The nonuniform displacements detected here do not resemble Jahn-Teller distortions as found for dopants on the Ti site [35–37]. Future Q-STEM studies of displacements in SrTiO<sub>3</sub> alloyed with other rare earth atoms or those having a different charge state (such as Eu<sup>+2</sup>) or no  $f$  electrons (such as La<sup>3+</sup>) should shed light on the electronic contributions to the observed displacements. We also note that the observed presence of local displacements is quite different from a previously investigated case of Sr dopants in SmTiO<sub>3</sub> [23], which only had a global effect on the structure. The fact that all three cases thus far (Sm-doped SrTiO<sub>3</sub>, Sr-doped SmTiO<sub>3</sub>, and SrTiO<sub>3</sub> containing Sr vacancies) have *quantitatively* different responses in their local structure to the presence of point defects highlights the importance of the Q-STEM technique in establishing structure-property relationships for these materials.

Finally, the complex structural disorder caused by the rare earth dopant atoms observed here may have implications for the properties of doped SrTiO<sub>3</sub>. For example, strained, doped SrTiO<sub>3</sub> can become simultaneously ferroelectric and superconducting [3,5]. Ferroelectricity in SrTiO<sub>3</sub> is a result of cooperative displacements of Ti atoms. A recent second harmonic generation study of the transition in strained doped SrTiO<sub>3</sub> showed that it could be described by an Ising model [5], which indicates a disorder-order component to the transition, in spite of the success of the softmode description for undoped, strained SrTiO<sub>3</sub> [38–40]. This raises interesting questions as to the influence of the preexisting displacements of Ti columns in doped SrTiO<sub>3</sub>, caused by the dopant atoms, on the nature of the ferroelectric transition, relative to that of undoped, strained SrTiO<sub>3</sub>.

### ACKNOWLEDGMENTS

The authors thank T. Schumann for the x-ray lattice parameter measurements and R. Seshadri for discussions. The microscopy work was supported by the U.S. Department of Energy (Grant No. DEFG02-02ER45994). Film growth experiments (K.A.) were supported by the National Science Foundation (Grant No. 1729489). We gratefully acknowledge the Center for Scientific Computing at the California Nanosystems Institute and the use of the MRL Shared Experimental Facilities, which are supported by the MRSEC Program of the U.S. National Science Foundation under Award No. DMR 1720256.

- 
- [1] J. F. Schooley, W. R. Hosler, E. Ambler, J. H. Becker, M. L. Cohen, and C. S. Koonce, Dependence of the Superconducting Transition Temperature on Carrier Concentration in Semiconducting SrTiO<sub>3</sub>, *Phys. Rev. Lett.* **14**, 305 (1965).
  - [2] C. W. Rischau, X. Lin, C. P. Grams, D. Finck, S. Harms, J. Engelmayer, T. Lorenz, Y. Gallais, B. Fauque, J. Hemberger, and K. Behnia, A ferroelectric quantum phase transition inside the superconducting dome of Sr<sub>1-x</sub>Ca<sub>x</sub>TiO<sub>3-δ</sub>, *Nat. Phys.* **13**, 643 (2017).
  - [3] K. Ahadi, L. Galletti, Y. T. Li, S. Salmani-Rezaie, W. Z. Wu, and S. Stemmer, Enhancing superconductivity in SrTiO<sub>3</sub> films with strain, *Sci. Adv.* **5**, eaaw0120 (2019).
  - [4] Y. Tomioka, N. Shirakawa, K. Shibuya, and I. H. Inoue, Enhanced superconductivity close to a non-magnetic quantum critical point in electron-doped strontium titanate, *Nat. Comm.* **10**, 738 (2019).
  - [5] R. Russell, N. Ratcliff, K. Ahadi, L. Dong, S. Stemmer, and J. W. Harter, Ferroelectric enhancement of superconductivity in compressively strained SrTiO<sub>3</sub> films, *Phys. Rev. Mater.* **3**, 091401(R) (2019).
  - [6] N. Mott, *Metal-Insulator Transitions* (Taylor & Francis, London, 1990).
  - [7] X. Lin, Z. W. Zhu, B. Fauque, and K. Behnia, Fermi Surface of the Most Dilute Superconductor, *Phys. Rev. X* **3**, 021002 (2013).
  - [8] E. Mikheev, B. Himmetoglu, A. P. Kajdos, P. Moetakef, T. A. Cain, C. G. Van de Walle, and S. Stemmer, Limitations to the room temperature mobility of two- and three-dimensional electron liquids in SrTiO<sub>3</sub>, *Appl. Phys. Lett.* **106**, 062102 (2015).
  - [9] X. Lin, B. Fauqué, and K. Behnia, Scalable T<sup>2</sup> resistivity in a small single-component Fermi surface, *Science* **349**, 945 (2015).
  - [10] E. Mikheev, S. Raghavan, J. Y. Zhang, P. B. Marshall, A. P. Kajdos, L. Balents, and S. Stemmer, Carrier density independent scattering rate in SrTiO<sub>3</sub>-based electron liquids, *Sci. Rep.* **6**, 20865 (2016).
  - [11] S. Stemmer and S. J. Allen, Non-Fermi liquids in oxide heterostructures, *Rep. Prog. Phys.* **81**, 062502 (2018).
  - [12] C. Collignon, X. Lin, C. W. Rischau, B. Fauque, and K. Behnia, Metallicity and superconductivity in doped strontium titanate, *Annu. Rev. Condens. Matter Phys.* **10**, 25 (2019).
  - [13] P. M. Mooney, Deep donor levels (DX centers) in III-V semiconductors, *J. Appl. Phys.* **67**, R1 (1990).
  - [14] A. Janotti, B. Jalan, S. Stemmer, and C. G. V. d. Walle, Effects of doping on the lattice parameter of SrTiO<sub>3</sub>, *Appl. Phys. Lett.* **100**, 262104 (2012).
  - [15] I. Yokota, Lattice distortion around charged impurity in semiconductors, *J. Phys. Soc. Jpn.* **19**, 1487 (1964).
  - [16] J. M. LeBeau, S. D. Findlay, L. J. Allen, and S. Stemmer, Quantitative Atomic Resolution Scanning Transmission Electron Microscopy, *Phys. Rev. Lett.* **100**, 206101 (2008).

- [17] H. Kim, J. Y. Zhang, S. Raghavan, and S. Stemmer, Direct Observation of Sr Vacancies in SrTiO<sub>3</sub> by Quantitative Scanning Transmission Electron Microscopy, *Phys. Rev. X* **6**, 041063 (2016).
- [18] J. Hwang, J. Y. Zhang, A. J. D'Alfonso, L. J. Allen, and S. Stemmer, Three-Dimensional Imaging of Individual Dopant Atoms in SrTiO<sub>3</sub>, *Phys. Rev. Lett.* **111**, 266101 (2013).
- [19] J. Y. Zhang, J. Hwang, B. J. Isaac, and S. Stemmer, Variable-angle high-angle annular dark-field imaging: application to three-dimensional dopant atom profiling, *Sci. Rep.* **5**, 12419 (2015).
- [20] R. Ishikawa, A. R. Lupini, S. D. Findlay, T. Taniguchi, and S. J. Pennycook, Three-dimensional location of a single dopant with atomic precision by aberration-corrected scanning transmission electron microscopy, *Nano Lett.* **14**, 1903 (2014).
- [21] J. M. Johnson, S. Im, Wolfgang Windl, and J. Hwang, Three-dimensional imaging of individual point defects using selective detection angles in annular dark field scanning transmission electron microscopy, *Ultramicroscopy* **172**, 17 (2016).
- [22] J. Feng, A. V. Kvit, C. Zhang, J. Hoffman, A. Bhattacharya, D. Morgan, and P. M. Voyles, Imaging of single La vacancies in LaMnO<sub>3</sub>, [arXiv:1711.06308](https://arxiv.org/abs/1711.06308).
- [23] H. Kim, P. B. Marshall, K. Ahadi, T. E. Mates, E. Mikheev, and S. Stemmer, Response of the Lattice Across the Filling-Controlled Mott Metal-Insulator Transition of a Rare Earth Titanate, *Phys. Rev. Lett.* **119**, 186803 (2017).
- [24] X. H. Sang, E. D. Grimley, C. N. Niu, D. L. Irving, and J. M. LeBeau, Direct observation of charge mediated lattice distortions in complex oxide solid solutions, *Appl. Phys. Lett.* **106**, 061913 (2015).
- [25] B. Jalan, R. Engel-Herbert, N. J. Wright, and S. Stemmer, Growth of high-quality SrTiO<sub>3</sub> films using a hybrid molecular beam epitaxy approach, *J. Vac. Sci. Technol. A* **27**, 461 (2009).
- [26] B. Jalan, P. Moetakef, and S. Stemmer, Molecular beam epitaxy of SrTiO<sub>3</sub> with a growth window, *Appl. Phys. Lett.* **95**, 032906 (2009).
- [27] J. M. LeBeau, S. D. Findlay, L. J. Allen, and S. Stemmer, Position averaged convergent beam electron diffraction: Theory and applications, *Ultramicroscopy* **110**, 118 (2010).
- [28] See Supplemental Material at <http://link.aps.org/supplemental/10.1103/PhysRevMaterials.3.114404> for PACBED patterns of the images analyzed in the main text, details of the image simulations, additional intensity data sets generated from multiple images, histograms of the displacement vectors, additional displacement vector maps for the 3% and 2% Sm-doped SrTiO<sub>3</sub>, and results for the number and depth positions of dopant atoms in columns A and B in Fig. 3.
- [29] P. Gao, A. Kumamoto, R. Ishikawa, N. Lugg, N. Shibata, and Y. Ikuhara, Picometer-scale atom position analysis in annular bright-field STEM imaging, *Ultramicroscopy* **184**, 177 (2017).
- [30] J. M. LeBeau and S. Stemmer, Experimental quantification of annular dark-field images in scanning transmission electron microscopy, *Ultramicroscopy* **108**, 1653 (2008).
- [31] J. M. LeBeau, S. D. Findlay, X. Q. Wang, A. J. Jacobson, L. J. Allen, and S. Stemmer, High-angle scattering of fast electrons from crystals containing heavy elements: Simulation and experiment, *Phys. Rev. B* **79**, 214110 (2009).
- [32] H. E. K. E. MacArthur, T. J. Pennycook, E. Okunishi, A. J. D'Alfonso, N. R. Lugg, L. J. Allen, and P. D. Nellist, Probe integrated scattering cross sections in the analysis of atomic resolution HAADF STEM images, *Ultramicroscopy* **133**, 109 (2013).
- [33] E. J. Kirkland, *Advanced Computing in Electron Microscopy*, 2nd ed. (Springer, New York, 2010).
- [34] S. Kobayashi, Y. Ikuhara, and T. Mizoguchi, Lattice expansion and local lattice distortion in Nb- and La-doped SrTiO<sub>3</sub> single crystals investigated by x-ray diffraction and first-principles calculations, *Phys. Rev. B* **98**, 134114 (2018).
- [35] H. J. d. Jong and M. Glasbeek, Cr<sup>5+</sup> in SrTiO<sub>3</sub>: An example of a static Jahn-Teller effect in a *d*<sup>1</sup> system, *Solid State Comm.* **19**, 1197 (1976).
- [36] T. W. Kool and M. Glasbeek, Electric field effects in EPR of the SrTiO<sub>3</sub> : V<sup>4+</sup> Jahn-Teller system, *J. Phys.: Condens. Matter.* **3**, 9747 (1991).
- [37] R. Evarestov, E. Blokhin, D. Gryaznov, E. A. Kotomin, R. Merkle, and J. Maier, Jahn-Teller effect in the phonon properties of defective SrTiO<sub>3</sub> from first principles, *Phys. Rev. B* **85**, 174303 (2012).
- [38] A. Antons, J. B. Neaton, K. M. Rabe, and D. Vanderbilt, Tunability of the dielectric response of epitaxially strained SrTiO<sub>3</sub> from first principles, *Phys. Rev. B* **71**, 024102 (2005).
- [39] H. Ma, J. Levy, M. D. Biegalski, S. Trolier-McKinstry, and D. G. Schlom, Room-temperature electro-optic properties of strained SrTiO<sub>3</sub> films grown on DyScO<sub>3</sub>, *J. Appl. Phys.* **105**, 014102 (2009).
- [40] A. K. Hamze and A. A. Demkov, First-principles study of the linear electro-optical response in strained SrTiO<sub>3</sub>, *Phys. Rev. Materials* **2**, 115202 (2018).